Inorganic Chemistry

Article

pubs.acs.org/IC

Synthesis of Hafnium Oxide-Gold Core–Shell Nanoparticles

Naween Dahal[†] and Viktor Chikan*[,‡]

[†]Department of Chemistry and Biochemistry, The University of Texas at Austin, University Station A5300, Austin, Texas 78712-0165, United States

[‡]Department of Chemistry, Kansas State University, Manhattan, Kansas 66506-0401, United States

Supporting Information

ABSTRACT: Developing cheap composite nanoparticle systems that combines a high dielectric constant with good conductivity is important for the future of the electronic industry. In this study, two different sizes, 7.3 ± 2.2 and 5.6 ± 1.9 nm, of HfO_2@Au core–shell nanoparticles are prepared by using a high-temperature reduction method. The core–shell nanoparticles are characterized by powder X-ray diffraction, high-resolution transmission electron microscopy (HRTEM), energy dispersive X-ray analysis (EDX), and UV–visible absorption spectroscopy. HfO_2 exhibits no absorption in the visible region, but the HfO_2@Au core–shell nanoparticles show a plasmon absorption band at 555 nm that is 25 nm red-shifted as compared to pure gold nanoparticles. According to transmission electron microscopy and energy dispersive X-ray analysis, the HfO_2 particles are coated with approximately three atomic layers of gold.

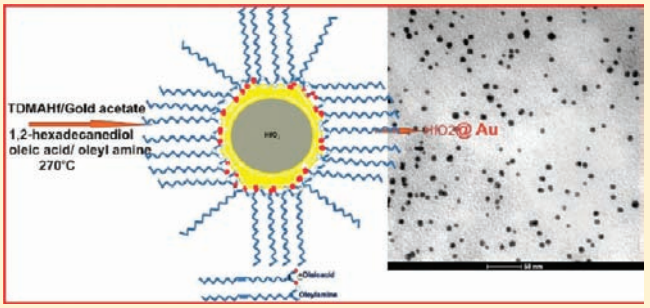

INTRODUCTION

Recently, the semiconductor industry has aimed at switching to hafnium-based transistors to replace polycrystalline silicon gate electrodes and silicon oxide-based insulators that are the core components of the transistors in integrated circuits. Because of reduced dimension, the thickness of the insulator (SiO_2) between source and drain approaches 1 nm. At this dimension, the leakage current approaches an unacceptable rate that results in power drainage and in overheating in the case of low-power devices such as cell phones and laptops.[1−4] To overcome this challenge, the search for high-κ dielectric materials has begun as the industry could no longer shrink the dielectric gate beyond the tunneling limit. In this regard, hafnium-based materials are considered the best alternatives for metal-gate electrodes,[4] and still making core–shell nanoparticles is not a matured process.

Both HfO_2 and gold have high dielectric constant values (≈25 and 6.9) respectively as compared to conventional silicon dioxide (3.9).[3−5] When these two materials are combined in a core–shell nanoparticle, the composite structure could allow new functionality. Without the addition of a Au shell, HfO_2 suffers from a high leakage current after high-temperature annealing (≥500 °C) due to the onset of crystallization.[2] This crystallization can be suppressed by the addition of a gold shell. Gold is a noble metal with a large work function value that ensures better charge retention and can be used in nanocrystalline-based nonvolatile floating gate memory.[1,3,6] As a result of the composite structure of HfO_2 and gold, the metal surface can be chemically modified in a highly controllable way because of gold affinity to various organic surfactants that form densely packed monolayers. Specifically, a key challenge for practical applications relies on developing gate dielectrics with low leakage current, low interface trap density, and high capacitance for low-voltage organic thin film transistors. Molecular self-assembled monolayers (SAMs) are excellent candidates in low-voltage gate dielectrics. SAMs are the densely packed organic molecular monolayers capable of suppressing carrier tunneling via highly ordered aliphatic chains despite the fact that they are only a few nanometers in thickness. In addition, because of the rich gold chemistry, tuning the terminal groups of SAMs and modifying the interface between the organic semiconductor and the dielectrics could result in improved device performance. In the literature, there are numerous examples of making SAMs on gold surfaces.[7−15] In addition, HfO_2@Au core–shell nanoparticles could find applications in the industry as a catalyst and heat resistant, highly reflective, and protective optical coating.[5] To the best of our knowledge, there is no report in the literature for the synthesis of HfO_2@Au core–shell nanoparticles despite their attractive applications. In this paper, a colloidal high-temperature reduction method is described to produce the HfO_2@Au nanoparticles.

EXPERIMENTAL SECTION

HfO_2@Au core–shell nanoparticles are synthesized by using a high-temperature reduction method.[7] In the first step, a HfO_2 seed solution is prepared by refluxing tetrakis dimethylaminohafnium(TDMAHf) (drybox) in the presence of 1,2-hexadecanediol. In the second step, the particles are coated with a gold shell. Both steps are carried out under inert atmosphere of argon. All chemicals are used as received;

Received: September 8, 2011
Published: December 16, 2011

   dx.doi.org/10.1021/ic201977d | *Inorg. Chem.* 2012, 51, 518–522

therefore, the water content in the chemicals is sufficient for the decomposition of tetrakis dimethylaminohafnium. The decomposition of this compound takes place according to this reaction:[16−18]

$$\mathrm{TDMAHf} + \mathrm{H_2O} \rightarrow \mathrm{HfO_2} + \mathrm{DMA}$$

The reaction is divided into two half-reactions:

$$\mathrm{Hf[N(CH_3)_2]_4} + \mathrm{Hf\text{-}OH} \rightarrow \mathrm{Hf\text{-}O\text{-}Hf[N(CH_3)_2]_3} + \mathrm{HN(CH_3)_2}$$

$$\mathrm{Hf\text{-}O\text{-}Hf[N(CH_3)_2]_3} + 3\mathrm{H_2O} \rightarrow \mathrm{Hf\text{-}O\text{-}Hf\text{-}OH_3} + 3\mathrm{HN(CH_3)_2}$$

In a typical synthesis, a solution containing HfO_2 nanoparticles is prepared from 0.2 mL of tetrakis dimethylaminohafnium (98%), 20 mL of dioctylether (99%), 1.5 mL of oleic acid (99%), 1.5 mL of oleylamine (70%), and 2.5 g of 1,2-hexadecanediol (90%). The solution is refluxed at 270 °C for 1.3 h. In the next step, 0.25 g of gold(III) acetate (99.9%), 2.5 g of 1,2-hexadecanediol, 1.5 mL of oleic acid, 2.5 mL of oleylamine, and 25 mL of dioctylether are added to 10 mL of solution of the HfO_2 nanoparticles. The solution is heated (at 15 °C/min) to 250 °C and refluxed for 2 h. Following this step, the solution is cooled to room temperature, and ethanol (99%) is added to precipitate the nanoparticles. The nanoparticle slur is centrifuged at 8000 rpm for 30 min. The dark purple precipitate containing the nanoparticles is deposited at the bottom of the centrifuge tube. After the precipitate is washed with ethanol four times, the nanoparticles are vacuum-dried at room temperature for 10 h. The dried nanoparticles are redispersed in hexane in the presence of 0.5 mL of oleic acid and 0.5 mL of oleyl amine. Size-selective precipitation is carried out by centrifuging and redissolving the nanoparticles in hexane or toluene.

Transmission electron microscopy (TEM) and high-resolution transmission electron microscopy (HRTEM) are performed on FEI Tecnai F20 XT field emission transmission electron microscope, schottky field emitter electron source, operated at 100 kV for low-resolution images and at 200 kV for high-resolution images. Powder X-ray diffraction (PXRD) patterns are recorded by a Bruker D8 X-ray diffractometer with Cu Kα radiation. Scanning electron microscopy (SEM) is performed on a Hitachi S-5500 operated at 30 keV equipped with an energy dispersive spectroscopy detector (Bruker EDS Quantax 4010) for the elemental mapping. The samples for the TEM, HRTEM, and SEM are prepared by drop casting the nanoparticles solution on the carbon-coated copper Formvar 200 mesh (Ted Pilla) grids and allowed to dry at room temperature. PXRD patterns are recorded with a Bruker AXS D8 diffractometer equipped with a Cu Kα radiation source (40 kV, 40 mA) with a step width of 0.018 (2θ) and an acquisition time of 0.2 s per step. UV−vis measurements are performed in five times diluted nanoparticles solution in 1 cm^3 quartz cuvette using the Ocean optics USB4000-UV−vis, preconfigured for applications from 200 to 850 nm. The nanoparticle sizes are calculated by using J-image, measuring the area of each nanoparticles in terms of pixel, obtained by averaging minimum and maximum pixels for 200 particles.

RESULTS AND DISCUSSION

Measurements of the surface plasmon resonance band of the nanoparticles indicate the formation of HfO_2@Au core−shell nanoparticles. Figure 1 shows the UV−visible absorption spectra of HfO_2@Au core−shell (square curve), gold (diamond curve), and HfO_2 seed nanoparticles (circle curve). The plasmon peak maximum of gold nanoparticles is located at 530 nm, and that of HfO_2@Au core−shell nanoparticles is at 555 nm. As expected, the plasmon peak of the HfO_2@Au core−shell nanoparticles shows 25 nm red shift as compared to gold nanoparticles prepared under identical conditions. There is no observation of plasmon peak of HfO_2 seeds nanoparticles

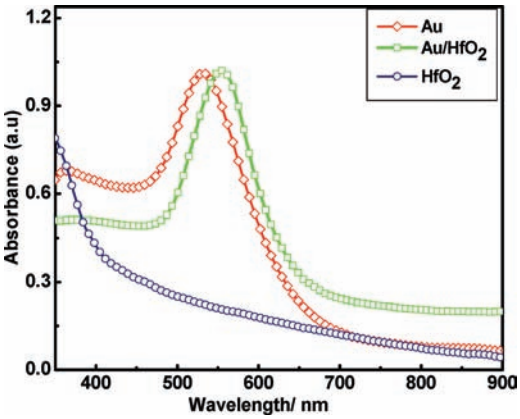

Figure 1. UV−visible absorption spectra of pure gold nanoparticles (diamond curve), HfO_2@Au core−shell nanoparticles (square curve), and bare hafnium oxide nanoparticles (circle curve).

in the visible region of the spectrum as represented in Figure 1. The surface plasmon resonance of core−shell nanoparticles depends upon the thickness of the shell, size, shape, and dielectric constant of immediate vicinity of the nanoparticles.[19−21] The red shift of the surface plasmon peak is due to a collective interaction of the electrons of the interconnected particles.[20,22,23] In this particular experiment, there is little shift in plasmon peak of HfO_2@Au core−shell nanoparticles despite the high dielectric constant of core material. The lack of plasmon peak shift suggests that the particles might have a thick shell of gold or the bulk dielectric constant of hafnium is not applicable. Usually, there is a concern of heterogeneous nucleation of gold particles independent from the HfO_2 particles. It is unlikely to have a significant amount of pure gold nanoparticles in these core−shell nanoparticle samples (see later TEM and XRD results) due to the lack of broadening of the surface plasmon peak.

Figure 2 shows the XRD spectra of pure gold nanoparticles (i), HfO_2@Au core−shell nanoparticles (ii), and HfO_2@Au

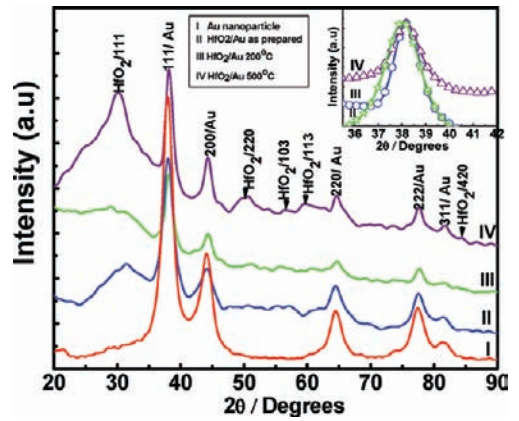

Figure 2. Powder XRD pattern of pure gold nanoparticles (i), XRD pattern of as prepared hafnium oxide-gold core−shell nanoparticles (ii), and XRD patterns of hafnium oxide-gold core shell annealed to 200 and 500 °C (iii and iv). The inset shows the shifting of (111) peak to higher 2θ while annealing the sample.

core−shell samples annealed at 200 and 500 °C (iii and iv). The XRD spectrum of the core−shell nanoparticles reveals that the samples are crystalline but not homogeneous. The 2θ angles at 37.9, 44.0, 64.5, 77.7, and 81.5° in Figure 2iii

dx.doi.org/10.1021/ic201977d | Inorg. Chem. 2012, 51, 518−522

correspond to (111), (200), (220), (311), and (222) fcc atomic reflection planes of core−shell nanoparticles. The XRD peaks of HfO_2@Au core−shell nanoparticles are located at similar 2θ angles, and the X-ray intensities are comparable to pure gold nanoparticles, in agreement with the gold shell of the nanoparticles. Therefore, the observation of well-developed fcc gold XRD pattern in HfO_2@Au core−shell nanoparticles confirms the presence of a highly crystalline gold shell. It is unlikely that the XRD provides conclusive results to determine the structure and chemical composition of both core and shell[24] because the metal shell could obstruct observation of diffraction peaks corresponding to hafnium oxide. When the samples are annealed at elevated temperature, the core and shell material undergoes changes. The inset of Figure 2 shows the changed in 2θ angle of (111) atomic reflections of core−shell nanoparticles at 25 °C (star curve) and after annealing at 200 and 500 °C (circle and triangle curve). Considerable change in 2θ angle (higher 2θ angle) is observed [from 37.94 to 38.24° 2θ for (111) atomic reflection] when the sample is annealed to 200 °C. Interestingly, no change in XRD peaks position is observed when the annealing temperature is increased from 200 to 500 °C. The observation indicates that the hafnia and gold of the nanoparticles alloyed with each other when annealed above 200 °C. The shifting of each peak position to higher 2θ values in the alloyed sample indicates softening of the lattice constant. It is speculated that this is due to the incorporation of gold into the hafnium oxide surface. The calculated average lattice constants for the alloy and pure gold nanoparticles for their cubic unit cell are 4.004 ± 0.025 and 4.064 ± 0.025 Å, respectively. The lattice constant of gold nanoparticles is very close to that of bulk gold (4.067 Å).[25] The XRD data show that there is no phase segregation of the elements in the core−shell nanoparticles below 200 °C (Figure S2 in the Supporting Information). At higher temperature (500 °C), the nanoparticles begin to crystallize, as proven by the appearance of the (111) peak of hafnium oxide as shown in Figure 2iv and Figure S3 in the Supporting Information.

Figure 3a shows the low-resolution TEM image of HfO_2@Au core−shell nanoparticles. The average sizes of the nanoparticles

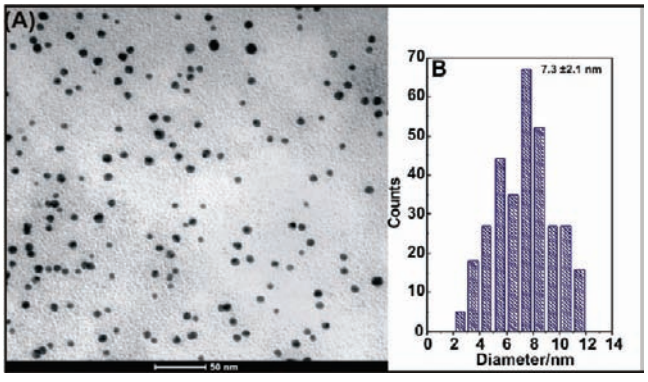

Figure 3. TEM image of as-prepared hafnium oxide-gold core−shell nanoparticles (A). The histogram shows the corresponding size distribution (B).

are 7.3 ± 2.1 nm as shown by the histogram in Figure 3b; however, the sizes of the hafnium oxide seeds are 3.7 ± 1.0 nm (Figure S1 in the Supporting Information). The TEM shows that the particles are multifaceted with irregular shape and mostly in the spherical form. Figure 4a represents the smaller

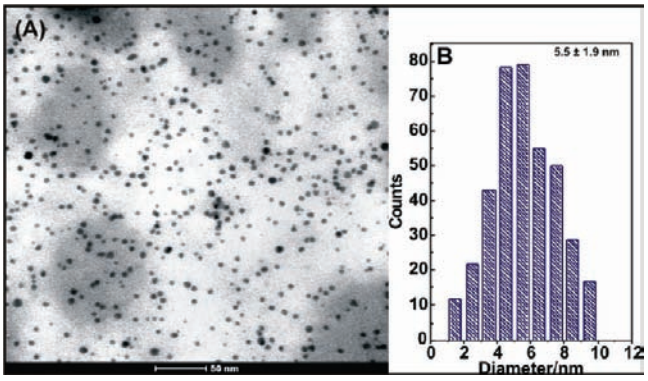

Figure 4. TEM image of hafnium oxide-gold core−shell nanoparticles after repetitive washing and centrifuging (A). The histogram shows the corresponding size distribution (B).

sizes of HfO_2@Au core−shell nanoparticles that are obtained by centrifuging the same batch of nanoparticles at 8000 rpm for 1.0 h and redissolving in hexane. The average size of the nanoparticles is 5.5 ± 1.9 nm, as represented by the histogram in Figure 4b. The particles are more aggregated and spherical due to centrifuging because the stabilizing double layer surrounding the nanoparticle is perturbed during centrifugation. Literature shows that centrifugation can induce polarization of the electrical double layer surrounding charged colloids.[26] Specifically, the lighter ions in the electrical double layer remain stationary relative to the downward movement of the particle, and the double layer becomes slightly polarized. Figure 5 shows the UV−visible absorption spectrum for large

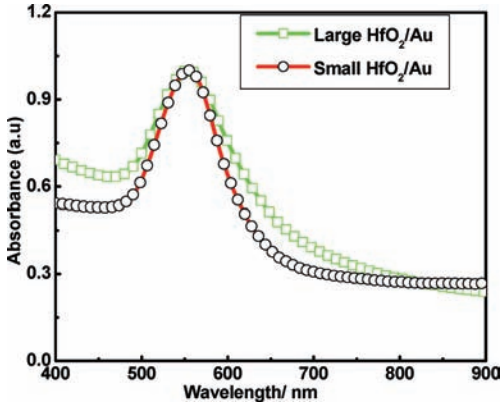

Figure 5. UV−visible absorption spectra of two different sizes of hafnium oxide-gold core−shell nanoparticles.

and small nanoparticles. The small nanoparticles are obtained after size selective precipitation as explained in Figure 4a. The size distribution of the large HfO_2@Au nanoparticles is larger as compared to the small nanoparticles. The full-width half-maximum of the large and small nanoparticles differs by 2.1 nm, which is very similar to the particle size measurements from the TEM. In addition, there is no shift in surface plasmon bands, but narrowing of the surface plasmon band of the smaller nanoparticles can be observed. This narrowing is the result of smaller HfO_2 core size and relatively thick gold shell. The smaller particles have a higher density that leads to the precipitation of these particles in the centrifuge first. These results show some limited ability to tune the size from the single batch synthesis of nanoparticles.

dx.doi.org/10.1021/ic201977d | *Inorg. Chem.* 2012, 51, 518−522

The structure of the HfO_2@Au core−shell nanoparticles is further studied by HRTEM and electron diffraction (Figure 6).

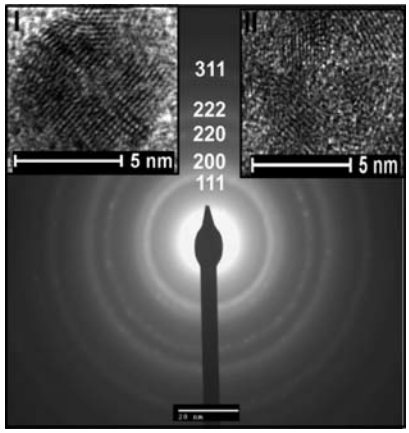

Figure 6. Electron diffraction of crystalline hafnium oxide-gold core−shell nanoparticles. The insets show selected HRTEM images of the core−shell structure of hafnium oxide-gold core−shell nanoparticles.

The insets I and II show the HRTEM images of HfO_2@Au core−shell nanoparticles. Multidomain structures with a regular lattice interplanar distances (0.24 nm), corresponding to fcc Au (111), are observed in both images. The particle size is very similar to that of low-resolution TEM measurement as in Figure 3c. The shell thickness of the nanoparticles calculated from the HRTEM analysis is 1.05 nm. The observation of several diffraction rings is attributed to the crystalline structure of the core−shell nanoparticles (Figure 6). The diffraction rings corresponding to the (111), (200), (220), (222), and (311) atomic reflection planes originate from the gold shell; the electron diffraction of the hafnium oxide core is shown in Figure S2 in the Supporting Information. The result is consistent with the powder XRD shown in Figure 2. Figure 7a shows a spectrum obtained from energy dispersive X-ray analysis (EDX) of HfO_2@Au core−shell nanoparticles containing approximately 20−25 nanoparticles area; a similar spectrum for the core hafnium oxide is also presented (see Figure S4 in the Supporting Information). Further confirmation of the core−shell structure is examined by the element mapping in the single particle basis. The presence of both hafnium and gold signal (figure 7b) in single particles and the corresponding EDX spectrum for single particles shown in Figure 7c further inferred the core−shell structure. The spectrum clearly shows the presence of both hafnium and gold in the nanoparticles. The atomic ratio of gold to hafnium from EDX analysis is found to be 81:19 (Table S1 in the Supporting Information). The thickness of the gold shell determined from the EDX data (see the Supporting Information) is found to be approximately 0.66 nm. Therefore, it is notable that the thickness calculated from the EDX analysis of the core−shell nanoparticles is within 33% accuracy to the thickness obtained from the TEM, which is 1.05 nm.

CONCLUSIONS

HfO_2@Au core−shell nanoparticles are successfully prepared by a high-temperature reduction method in solution. The growth of such structures is based on the seeded nucleation of gold on the surface of hafnium oxide. It is expected that the flexible gold chemistry of the HfO_2@Au dielectrics allows

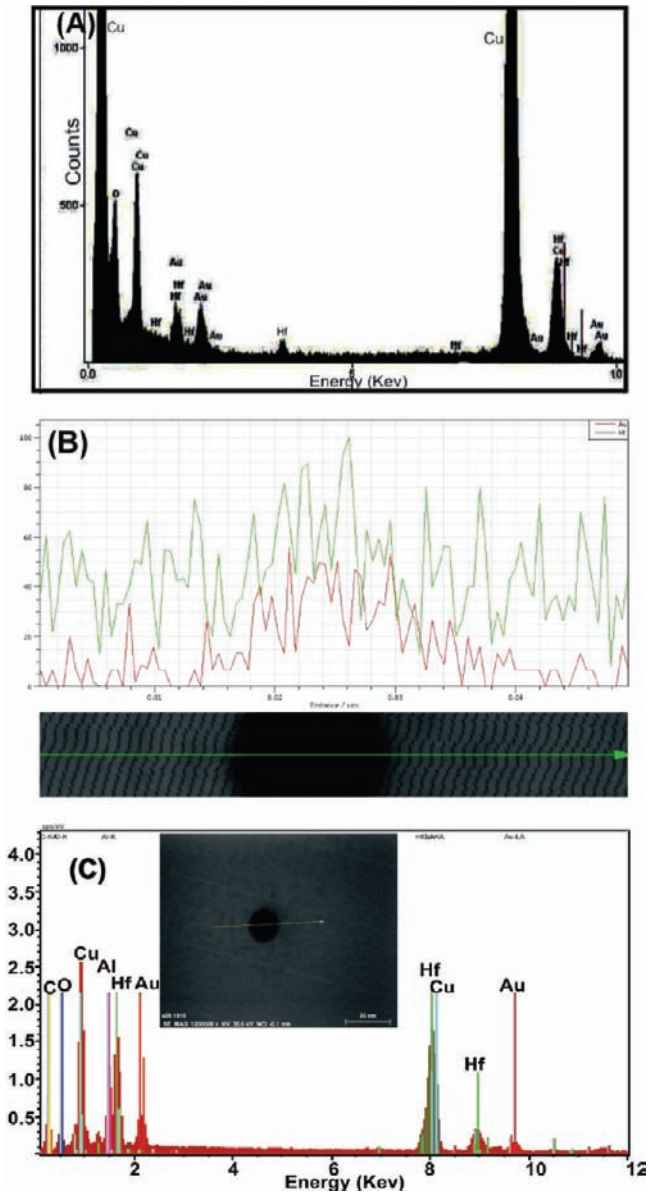

Figure 7. (A) Energy dispersive X-ray spectrum of hafnium oxide-gold core−shell nanoparticles for large area measurements. (B) Line scan mapping for hafnium (green) and gold (red) and the corresponding particle at the bottom of the figure. (C) Energy dispersive X-ray spectrum of a hafnium oxide-gold core−shell nanoparticle; the inset shows the corresponding nanoparticle.

better processing for SAM formation as compared to SiO_2. High-quality, high-κ HfO_2@Au can be prepared by a quick and simple solution processing and be easily modified by several organic SAMs. The preparation and characterization of SAMs with HfO_2@Au nanoparticles are the future goal of this research.

ASSOCIATED CONTENT

Supporting Information

XRPD data for HfO_2 seeds as prepared and annealed at 200 and 500 °C, TEM image and corresponding size histogram, electron diffraction, compositions for both HfO_2 and HfO_2@Au from EDX measurements, and shell thickness calculation from the EDX data. This material is available free of charge via the Internet at http://pubs.acs.org.

dx.doi.org/10.1021/ic201977d | *Inorg. Chem.* 2012, 51, 518−522

AUTHOR INFORMATION

Corresponding Author

*E-mail: chikan@ksu.edu.

ACKNOWLEDGMENTS

We are grateful to the Department of Chemistry at Kansas State University for funding and the University of Kansas for the Microscope facilities for the opportunity to obtain high-quality TEM images and for the help of the staff. We thank Dr. Anthony Dylla for assistance with SEM-EDX experiments.

REFERENCES

(1) Zhu, X. H.; Zhu, J. M.; Li, A. D.; Liu, Z. G.; Ming, N. B. *J. Mater. Sci. Technol.* **2009**, *25*, 289−313.
(2) Chen-Chan, W.; Jyun-Yi, W.; Yan-Kai, C.; Che-Hao, C.; Tai-Bor, W. *Appl. Phys. Lett.* **2007**, *91*, 202110.
(3) Jung Yup, Y.; Ju Hyung, K.; Won Joon, C.; Young Ho, D.; Chae Ok, K.; Jin Pyo, H. *J. Appl. Phys.* **2006**, *100*, 066102.
(4) Matthews, J. *Physics Today* **2008**, February.
(5) Tang, J.; Fabbri, J.; Robinson, R. D.; Zhu, Y.; Herman, I. P.; Steigerwald, M. L.; Brus, L. *EChem. Mater.* **2004**, *16*, 1336−1342.
(6) Groeseneken, G.; Aoulaiche, M.; De Gendt, S.; Degraeve, R.; Houssa, M.; Kauerauf, T.; Pantisano, L. *Reliability Issues in Advanced High k/Metal Gate Stacks for 45 nm CMOS Applications*, Advanced Semiconductor Devices and Microsystems, ASDAM '06. International Conference on 2006; pp 15−19.
(7) Song, S.; Clark, R. A.; Bowden, E. F.; Tarlov, M. J. *J. Phys. Chem.* **1993**, *97*, 6564−6572.
(8) Laibinis, P. E.; Whitesides, G. M.; Allara, D. L.; Tao, Y. T.; Parikh, A. N.; Nuzzo, R. G. *J. Am. Chem. Soc.* **1991**, *113*, 7152−7167.
(9) Park, J. W. *Bull. Korean Chem. Soc.* **2010**, *31*, 2861−2866.
(10) Grabar, K. C.; Freeman, R. G.; Hommer, M. B.; Natan, M. J. *Anal. Chem.* **1995**, *67*, 735−743.
(11) Freeman, R. G.; Grabar, K. C.; Allison, K. J.; Bright, R. M.; Davis, J. A.; Guthrie, A. P.; Hommer, M. B.; Jackson, M. A.; Smith, P. C.; Walter, D. G.; Natan, M. J. *Science* **1995**, *267*, 1629−1632.
(12) Tour, J. M.; Jones, L.; Pearson, D. L.; Lamba, J. J. S.; Burgin, T. P.; Whitesides, G. M.; Allara, D. L.; Parikh, A. N.; Atre, S. V. *J. Am. Chem. Soc.* **1995**, *117*, 9529−9534.
(13) Love, J. C.; Estroff, L. A.; Kriebel, J. K.; Nuzzo, R. G.; Whitesides, G. M. *Chem. Rev.* **2005**, *105*, 1103−1169.
(14) Sellers, H.; Ulman, A.; Shnidman, Y.; Eilers, J. E. *J. Am. Chem. Soc.* **1993**, *115*, 9389−9401.
(15) Bryant, M. A.; Pemberton, J. E. *J. Am. Chem. Soc.* **1991**, *113*, 8284−8293.
(16) Hausmann, D. M.; Kim, E.; Becker, J.; Gordon, R. G. *Chem. Mater.* **2002**, *14*, 4350−4358.
(17) Cho, M. J.; Jeong, D. S.; Park, J.; Park, H. B.; Lee, S. W.; Park, T. J.; Hwang, C. S.; Jang, G. H.; Jeong, J. *Appl. Phys. Lett.* **2004**, *85*, 5953−5955.
(18) Cho, M.; Park, H. B.; Park, J.; Lee, S. W.; Hwang, C. S.; Jang, G. H.; Jeong, J. *Appl. Phys. Lett.* **2003**, *83*, 5503−5505.
(19) Wang, L. Y.; Luo, J.; Maye, M. M.; Fan, Q.; Qiang, R. D.; Engelhard, M. H.; Wang, C. M.; Lin, Y. H.; Zhong, C. J. *J. Mater. Chem.* **2005**, *15*, 1821−1832.
(20) Moores, A.; Goettmann, F. *New J. Chem.* **2006**, *30*, 1121−1132.
(21) Miller, M. M.; Lazarides, A. A. *J. Phys. Chem. B* **2005**, *109*, 21556−21565.
(22) Shevchenko, E. V.; Bodnarchitk, M. I.; Kovalenko, M. V.; Talapin, D. V.; Smith, R. K.; Aloni, S.; Heiss, W.; Alivisatos, A. P. *Adv. Mater.* **2008**, *20*, 4323−4329.
(23) Radloff, C.; Halas, N. J. *Nano Lett.* **2004**, *4*, 1323−1327.
(24) Zhang, J.; Post, M.; Veres, T.; Jakubek, Z. J.; Guan, J.; Wang, D.; Normandin, F.; Deslandes, Y.; Simard, B. *J. Phys. Chem. B* **2006**, *110*, 7122−7128.
(25) Dahal, N.; Chikan, V.; Jasinski, J.; Leppert, V. J. *Chem. Mater.* **2008**, *20*, 6389−6395.
(26) Roca, M.; Pandya, N. H.; Nath, S.; Haes, A. J. *Langmuir* **2009**, *26*, 2035−2041.